Copyright Warning & Restrictions

The copyright law of the United States (Title 17, United States Code) governs the making of photocopies or other reproductions of copyrighted material.

Under certain conditions specified in the law, libraries and archives are authorized to furnish a photocopy or other reproduction. One of these specified conditions is that the photocopy or reproduction is not to be "used for any purpose other than private study, scholarship, or research." If a, user makes a request for, or later uses, a photocopy or reproduction for purposes in excess of "fair use" that user may be liable for copyright infringement,

This institution reserves the right to refuse to accept a copying order if, in its judgment, fulfillment of the order would involve violation of copyright law.

Please Note: The author retains the copyright while the New Jersey Institute of Technology reserves the right to distribute this thesis or dissertation

Printing note: If you do not wish to print this page, then select "Pages from: first page # to: last page #" on the print dialog screen

ABSTRACT

MAGNETIC IRON OXIDE NANOPARTICLES: SYNTHESIS, CHARACTERISTICS, MAGNETIC BEHAVIOR, AND BIOMEDICAL APPLICATIONS

by
Chengyin Fu

Magnetic iron oxide nanoparticles are attracting increasing attention due to their interesting properties that can be applied in a great number of applications such as catalysis and biomedicine. This thesis focuses on the synthesis, characteristics, and biomedical applications of iron oxide nanoparticles. The two most common iron oxides, including magnetite and maghemite, are discussed in this thesis.

For most of their applications, the magnetic behavior of iron oxide nanoparticles in a fluid is very important, especially, the high gradient magnetic separation of the particles from a nonmagnetic liquid medium, such as blood in the human body. A 2D model, which represents a slice through the center of a spherical particle in a fluid, is created in this thesis, and only the magnetic force and the drag force are taken into consideration. The magnetization of the particle is calculated by using the Langevin function, and the fluid drag force is calculated by using the Navier–Stokes equation. The trajectory function for this model is calculated, and the trajectories are drawn for specific cases.

MAGNETIC IRON OXIDE NANOPARTICLES: SYNTHESIS, CHARACTERISTICS, MAGNETIC BEHAVIOR, AND BIOMEDICAL APPLICATIONS

by
Chengyin Fu

A Thesis
Submitted to the Faculty of
New Jersey Institute of Technology
in Partial Fulfillment of the Requirements for the Degree of
Master of Science in Materials Science and Engineering

Interdisciplinary Program in Materials Science and Engineering

May 2012

APPROVAL PAGE

MAGNETIC IRON OXIDE NANOPARTICLES: SYNTHESIS, CHARACTERISTICS, MAGNETIC BEHAVIOR, AND BIOMEDICAL APPLICATIONS

Chengyin Fu

Dr. N.M. Ravindra, Thesis Advisor — Date
Professor of Physics, NJIT

Dr. Ken Ahn, Committee Member — Date
Assistant Professor of Physics, NJIT

Dr. Michael Jaffe, Committee Member — Date
Research Professor of Biomedical Engineering, NJIT

BIOGRAPHICAL SKETCH

Author: Chengyin Fu

Degree: Master of Science

Date: May 2012

Undergraduate and Graduate Education:

- Master of Science in Materials Science and Engineering, New Jersey Institute of Technology, Newark, NJ, 2012
- Bachelor of Science in Materials Science and Engineering, Tongji University, Shanghai, P. R. China, 2008

Major: Materials Science and Engineering

To people that I love.
To people that love me.
You make my life wonderful.

ACKNOWLEDGMENT

I would like to express the deepest appreciation to my thesis advisor, Dr. N.M. Ravindra. Without his guidance and persistent help this thesis would not have been possible.

I would like to thank Dr. Ken Ahn and Dr. Michael Jaffe for being part of my thesis review committee and for providing suggestions and guidance for my research.

I would like to thank Dr. N.M Ravindra for his valuable suggestion and great help in my study in NJIT.

Finally, I would like to thank my parents, who have been supportive to me during my life. Thank you for their greatest love.

TABLE OF CONTENTS

TABLE OF CONTENTS
(Continued)

Chapter **Page**

LIST OF TABLES

LIST OF FIGURES

CHAPTER 1

INTRODUCTION

Nanoscience is the study of matters whose size is on the nanometer scale. Comparing to the bulk materials, the materials on nanoscale have many unusual properties such as electrical, optical, and magnetic properties. Iron oxide nanoparticles are iron oxide particles with diameters between 1 and 100 nanometers. They have attracted much attention due to their fine magnetic properties and massive fields of applications in modern science.

The most common iron oxides in nature and biomedical applications are magnetite (Fe_3O_4) and maghemite (γ-Fe_2O_3), so they are also the subject of this thesis. The physical propertied of them are listed in Table 1.1.

Table 1.1 Physical Properties of Iron Oxides [1]

Properties	**Magnetite (Fe_3O_4)**	**Maghemite (γ-Fe_2O_3)**
Density (g/cm^3)	5.18	4.87
Melting point (°C)	1583-1597	-
Hardness	5.5	5
Type of magnetism	Ferromagnetic	Ferromagnetic
Curie temperature (K)	850	820-986
M_s at 300K ($A\text{-}m^2/kg$)	92-100	60-80
Standard free energy of formation $\Delta G_f°$ (kJ/mol)	-1012.6	-711.1
Crystallographic system	Cubic	Cubic or tetrahedral
Structural type	Inverse spinel	Defect spinel
Space group	Fd3m	$P4_332$ (cubic); $P4_12_12$ (tetragonal)
Lattice parameter (nm)	a = 0.8396	a = 0.83474 (cubic); a = 0.8347, c = 2.501 (tetragonal)

Magnetite is a black magnetic mineral and also called iron(II,III) oxide or ferrous ferrite. The molecular formula, Fe_3O_4, can also be written as $FeO \bullet Fe_2O_3$, which consists of wüstite (FeO) and hematite (Fe_2O_3). It has the strongest magnetism of all the natural minerals existing on the Earth [2]. Maghemite is a brown magnetic mineral, which occurs in soils. It exhibits strong magnetism, and it is metastable with respect to hematite and forms a continuous metastable solid solution with magnetite [3].

Magnetite and maghemite have the same crystal structure. The iron and oxygen ions form a face-centered cubic crystal system, and the oxygen ions are in the cubic close-packed arrangement (Figure 1.1). Magnetite has an inverse spinal structure, and Fe^{3+} ions occupy all the tetrahedral sites and both Fe^{3+} and Fe^{2+} ions occupy all the octahedral sites. Maghemite has a spinal structure. Differing with magnetite, vacancies exist in the octahedral sites in maghemite, and Fe^{3+} ions occupy two-third of the sites. One unit cell of maghemite contains 32 oxygen ions, $21\ \frac{1}{3}\ Fe^{3+}$ ions, and $2\ \frac{1}{3}$ vacancies.

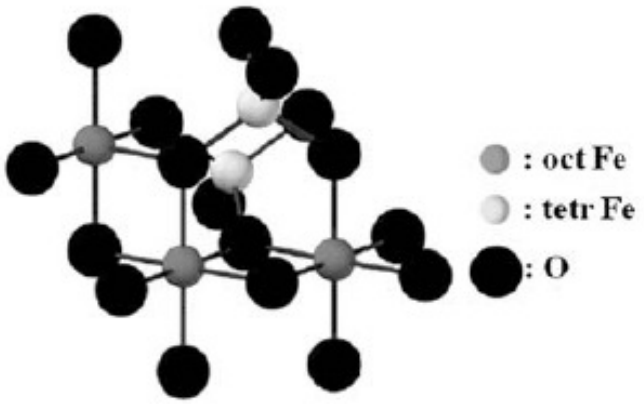

Figure 1.1 Crystal structure of magnetite and maghemite [1].

CHAPTER 2

BASIC MAGNETIC PROPERTIES OF IRON OXIDE NANOPARTICLES

Iron atom has four unpaired electrons in 3d orbital, so it has a strong magnetic moment. Fe^{3+} ions have five unpaired electrons in 3d orbital, and Fe^{2+} ions have four. When crystals are formed from iron atoms or Fe^{3+} and Fe^{2+} ions, they can be in ferromagnetic, antiferromagnetic or ferrimagnetic states [4].

In the paramagnetic state, all the magnetic moments are randomly oriented, so the crystal has a zero net magnetic moment (Figure 2.1). The crystal has a small net magnetic moment when an external magnetic field is applied, and the magnetic moment is zero when the field is removed. In a ferromagnetic crystal, all the magnetic moments are aligned even without an external magnetic field. In a ferrimagnetic crystal, two types of atoms with different magnetic moments are aligned in an antiparallel fashion, and the antiparallel moments have different magnitudes. The crystal is antiferromagnetic if the antiparallel moments have the same magnitudes. Both magnetite and maghemite are ferrimagnetic.

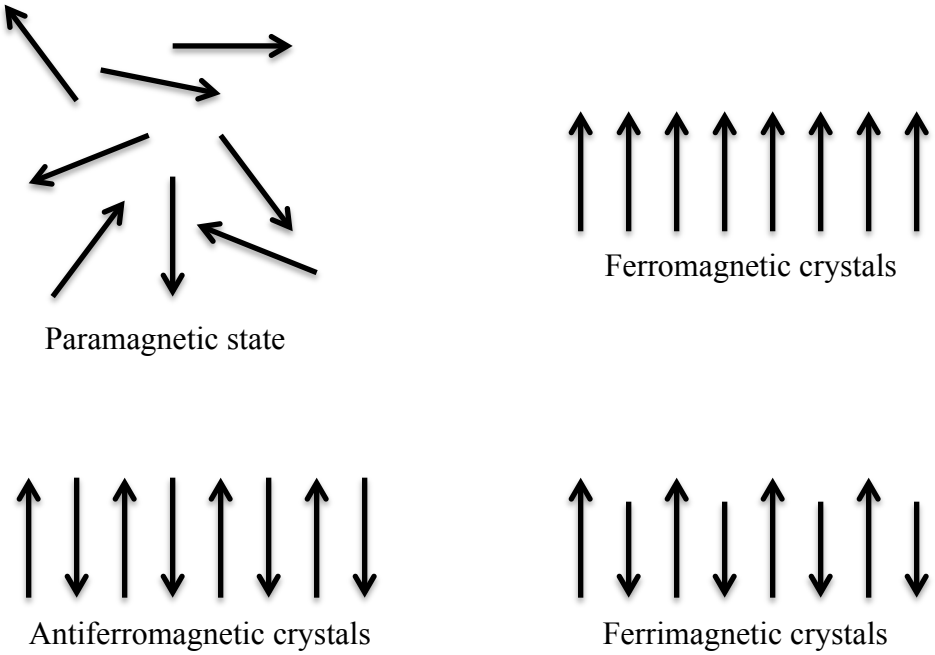

Figure 2.1 The magnetic spin alignments in different types of crystals.

The magnetization, M, represents the net magnetic moment per unit volume that is aligned parallel to the external field. The magnitude of M is generally less than the value when all the magnetic moments are perfectly aligned because different magnetic domains exit in crystal (Figure 2.2). In each domain, the magnetic moments are perfectly aligned. However, the moments of all domains are usually not aligned, so the magnetization decreases.

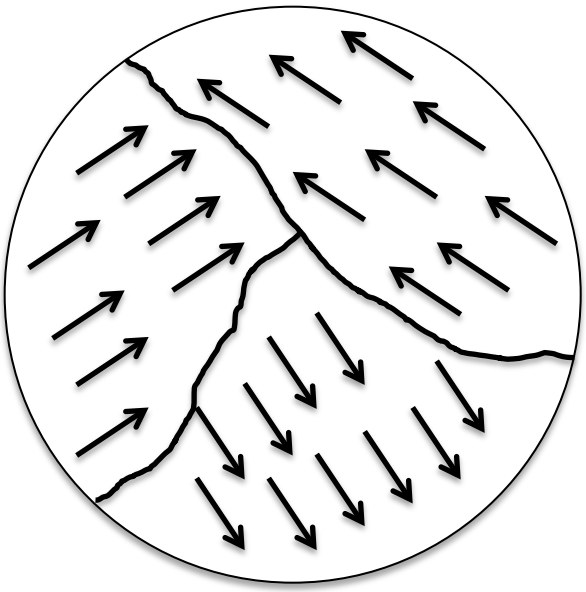

Figure 2.2 Magnetic domains in a crystal.

When an external magnetic field, H, is applied to a crystal, the crystal has a magnetization, M (Figure 2.3). M increases with the increase of H until it reaches its maximum value called saturation magnetization, M_s. When the field is removed, there is still a nonzero magnetization called remnant magnetization, M_r. To bring the magnetization back to zero, a coercivity field, H_c, must be applied in an antiparallel fashion. The diagram of this relation is called a hysteresis loop.

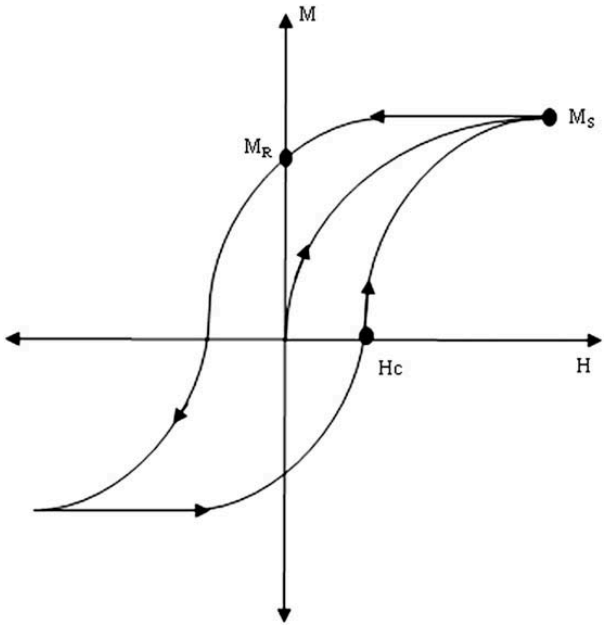

Figure 2.3 The Hysteresis loop.

When the size of the crystal decreases, the number of domains decreases as well. The crystal becomes a single domain when the size is blow some critical value. A single domain magnetic crystal has no hysteresis loop; it is superparamagnetic, which means it demagnetizes completely (M=0) when the field is removed. Iron oxide nanoparticles smaller than about 20 nm often display superparamagnetic behavior at room temperature [1].

The degree of alignment of magnetic moments is a function of temperature. The alignment is more disordered when the temperature increases, and beyond a critical temperature, the magnetization of the crystal becomes zero. For both magnetite and maghemite, the critical temperature is called Curie temperature, T_C. Superparamagnetic particles are different from this normal behavior; it occurs when the temperature is below a blocking temperature T_B.

Magnetite has a Curie temperature of 850 K [5]. At room temperature, magnetic particles that are smaller than 6 nm are superparamagnetic [6]. Their magnetic properties strongly depend on their synthesis method [7,8] and crystal morphology [9,10].

Maghemite has a phase transformation temperature of 400 °C above which it changes to hematite. Therefore, the Curie temperature of it is difficult to measure. However, the temperature is believed to be between 820 K and 986 K [1]. At room temperature, maghemite particles that are smaller than 10 nm are superparamagnetic [11].

Due to the very small size of the particles, the surface atoms have a very large percentage of all the atoms. Therefore, the surface effects are very important for nanoparticles. For the same material, the magnetization of small particles can be smaller than that of bulk materials. This reduction has been associated with different mechanisms, such as the existence of a magnetically dead layer on the surface of the particles, the existence of canted spins, or the existence of a spin-glass-like behavior of the surface spins [12]. Surface modifications are also very influential to the magnetic properties of the particles [13,14].

CHAPTER 3

SYNTHESIS OF PARTICLES

The preparation method has a very large effect on the size, shape, size distribution, and surface chemistry of the magnetic nanoparticles and also on their applications [15]. To synthesize the magnetic nanoparticles with customized size and shape has been always a challenge. Many synthesis methods have been developed to attain the desired particles; Figure 3.1 shows the three most important published routes of the preparation methods. Chemical synthesis has been the most common route, and almost 90% of the published work (up to date) is on this subject. In addition, the most common method of synthesis is the coprecipitation technique of iron salts.

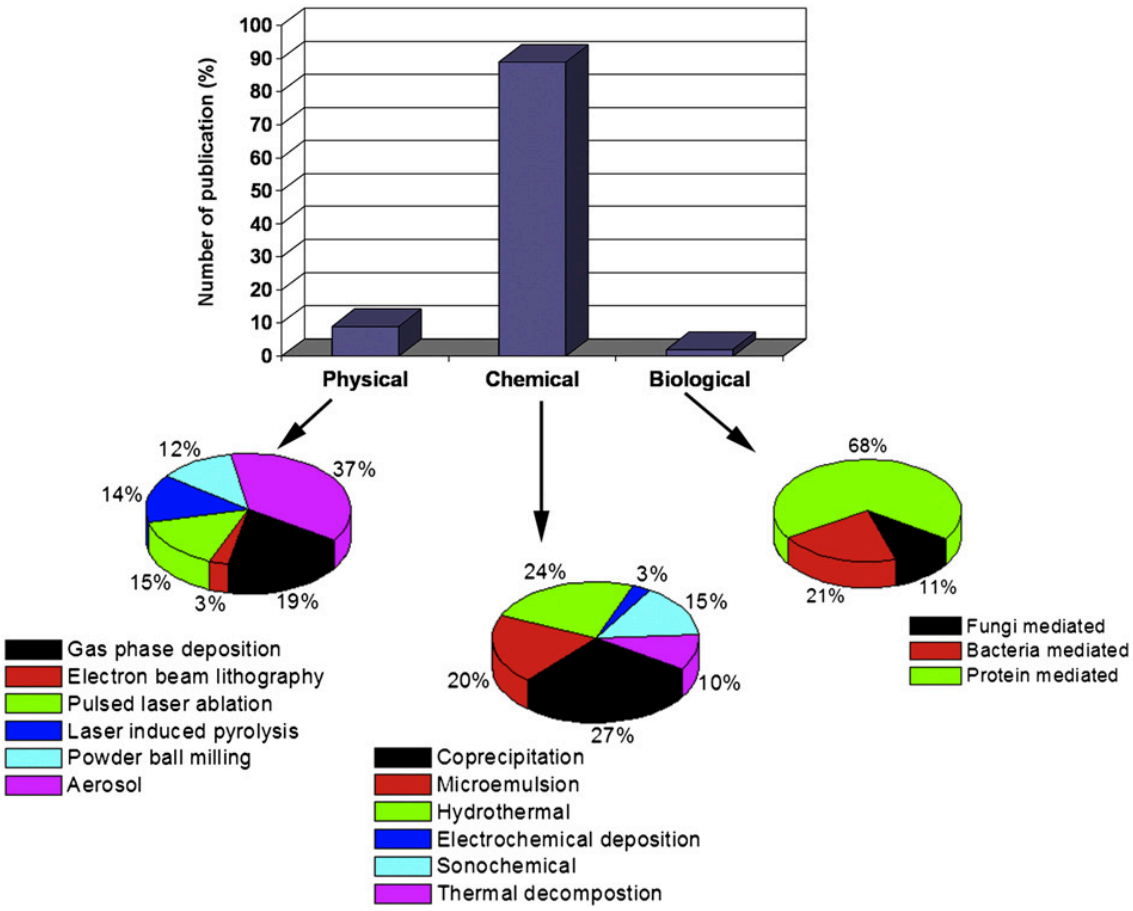

Figure 3.1 A comparison of published work on the synthesis of magnetic nanoparticles by three different routes [16].

3.1 Coprecipitation

The coprecipitation method is the most promising due to its simplicity and productivity [17]. It is widely used in biomedical applications because of ease of implementation and need for less hazardous materials and procedures [18]. In this method, iron oxide particles are produced by an ageing stoichiometric mixture of ferrous and ferric salts in aqueous media [19]. The size, shape, and composition of the particles depend on the salts used, the Fe^{3+} and Fe^{2+} ratio, the pH of the solution, the temperature, and the ionic strength of the media [20].

The chemical reaction of Fe_3O_4 formation can be written as:

$$Fe^{2+} + 2OH^- \rightarrow Fe(OH)_2$$

$$Fe^{3+} + 3OH^- \rightarrow Fe(OH)_3$$

$$Fe(OH)_2 + 2\,Fe(OH)_3 \rightarrow Fe_3O_4 + 4H_2O$$

According to the thermodynamics of this reaction, a complete precipitation of Fe_3O_4 should be expected between pH 9 and 14, while maintaining a molar ratio of Fe^{3+}:Fe^{2+} is 2:1 under a non-oxidizing oxygen-free environment [21]. Fe_3O_4 is not very stable, and it can be oxidized into γ-Fe_2O_3 in the presence of oxygen. The reaction can be written as:

$$Fe_3O_4 + 0.25O_2 + 4.5H_2O \rightarrow 3Fe(OH)_3$$

$$2Fe(OH)_3 \rightarrow \gamma\text{-}Fe_2O_3 + 3H_2O$$

To prevent this oxidation in air, an oxygen-free environment is very important. Nitrogen is used to produce such environment by passing through the solution. The nitrogen through the solution not only can prevent the oxidation but also reduces the particles size [22, 23].

There are two steps in the coprecipitation process. Small nuclei are first formed in the medium when the concentration of the species reaches critical supersaturation, and it is followed by the growth of the crystal. In the later step, the solutes diffuse to the surface of the crystal, and the process is controlled by the mass transport. The two steps need to be separated for producing nanoparticles. For example, the nucleation should not occur during the crystal growth step [24].

The nucleation and the crystal growth steps are illustrated in the LaMer diagram (Figure 3.2). In the supersaturated solution, if the nuclei are formed at the same time, the particles can have a very small size distribution after crystal growth. Therefore, the

nucleation process usually needs to be accomplished in a very short period of time for small size distribution of the particles. In addition, the number of particles is determined by the end of the nucleation process and not changing during the crystals growth.

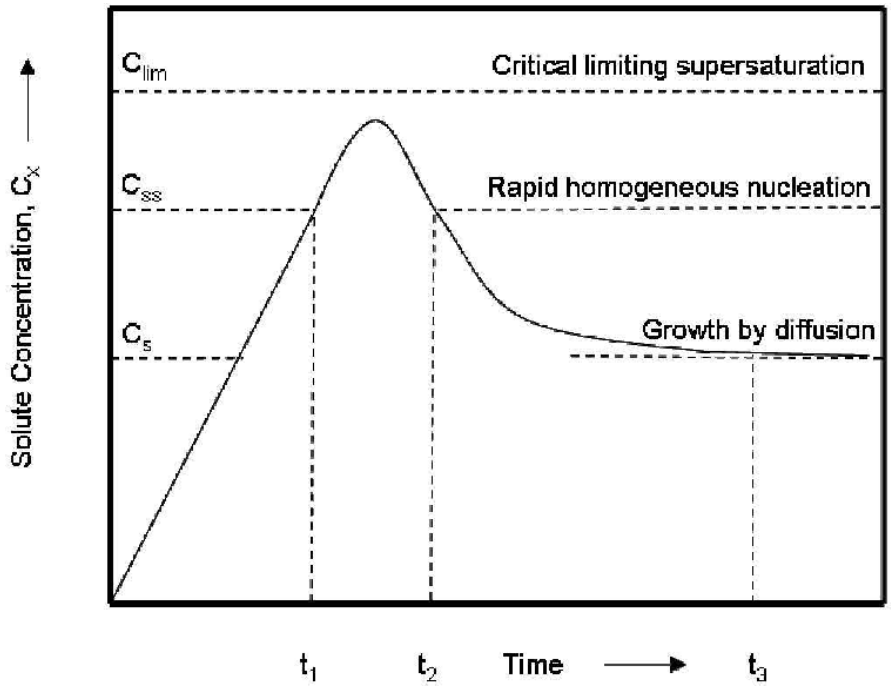

Figure 3.2 The LaMer Diagram [24].

Adding chelating organic anions (carboxylate or α-hydroxy carboxylate ions, such as gluconic, citric, or oleic acid) or polymer surface complexing agents (dextran, polyvinyl alcohol, or starch) during the formation of magnetite nanoparticles can help to control their size. The addition of organic ions can inhibit either nucleation or crystal growth according to the ratio between organic ions and iron salts, which means they can either lead to larger or smaller particles.

The Sugimoto's method was a very well established synthesis method, which was reported in 1980 [25]. In this method, ferrous salt is used in the presence of KNO_3 and KOH.

The most common synthesis method is the Massart's method, which was reported in 1981. In the method, $FeCl_3$ and $FeCl_2$ are used in alkali to produce the nanoparticles [26]. For magnetite synthesis, Sugimoto's method produces larger particles (30 to 200 nm), and Massart's method produces smaller particles (<20 nm) (Figure 3.3) [27].

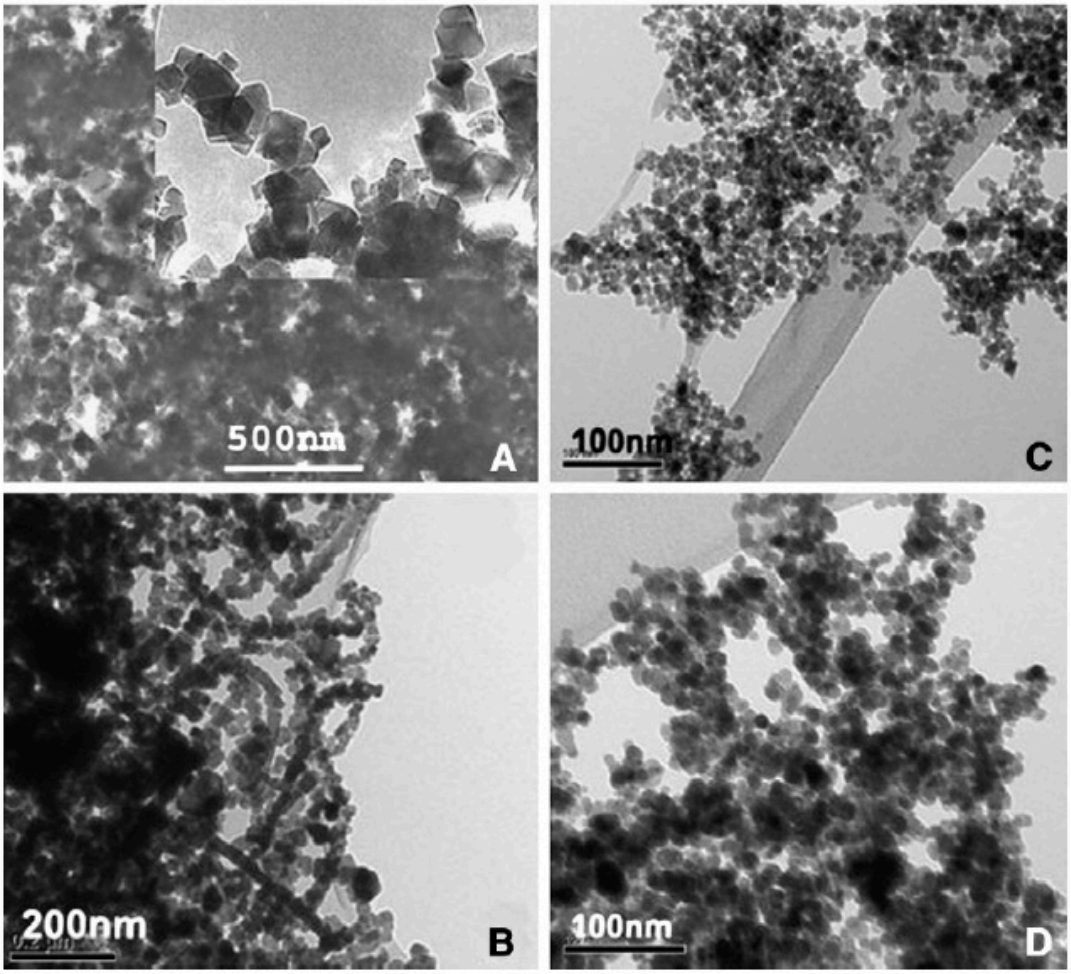

Figure 3.3 TEM micrographs of magnetite nanoparticles: A. Prepared by Sugimoto's method reaction in the presence of excess [OH^-]; B. Prepared by Sugimoto's method reaction without stirring and without excess of [OH^-] or [Fe^{2+}]; C. Prepared by Massart's method reaction in the presence of NH_4OH; D. Prepared by Massart's method reaction in the presence of dispersing agent TMAOH and without NH_4OH [27].

In the original Massart's method, the spherical magnetite particles have a diameter of 8 nm. The influence of the base (NaOH, ammonia, and CH_3NH_2), the pH, the cations added (Na^+, Li^+, K^+, NH_4^+, $N(CH_3)_4$, and $CH_3NH_3^+$), and Fe^{3+} and Fe^{2+} ratio on the productivity and size of the nanoparticles were studied in the Massart's report. By

adjusting all the parameters, the particles with size ranging from 4.2 to 16.6 nm can be produced [19]. In other reports, the influence of pH and ionic strength were studied, and particles with size ranging from 2 to 15 nm were produced. In addition, the two parameters affect the surface composition of the nanoparticles, which means that they also influence the electronic surface charge of the particles. The shape of the particles is related to the electronic surface density of the nanoparticles [28,29]. The medium can be either aqueous media or nonpolar liquids (oil or organic solvents) [30]. In another process reported by Massart [31], γ-Fe_2O_3 were produced by a rapid synthesis method, and the method allowed various coatings, such as α-hydroxyacids, amino acids, hydroxamate, phosphoryl choline, or dimercaptosuccinic acid.

The influence of Fe^{2+} and Fe^{3+} ratio (x) on the particles size, shape, composition, and magnetic properties has been studied [32]. When the ratio is too small, FeO(OH) forms in the solution. When x=0.3, there are two phases coexisting. One has a Fe^{2+} and Fe^{3+} ratio of 0.07 and produces 4 nm particles; the other has a ratio of 0.33 and produces larger particles. When x=0.35, only one phase exists. When x=0.5, the particles are homogeneous in size and chemical composition.

The iron concentration is also an important factor of synthesis. The optimized concentration is between 39 and 78 millimolar.

The pH and ionic strength has a large influence on the size of the particles. Due to their effect on the electrostatic surface charge, the particle size and size distribution width decreases when pH and ionic strength are increased [24].

In Qiu's report, the influence of ionic strength on the nanoparticles was carefully studied [33]. The ionic strength is changed by adding 1 M NaCl solution. The magnetite

particles with size 1.5 nm are attained in the report, and they are smaller than the particles formed when there is no added NaCl. In addition, in the solution with higher ionic strength, the formed particles also have lower saturation magnetization (63 emu/g) than that of normal particles (71 emu/g).

The mixing rate also influence the size of the particles. When the mixing rate increases, the size of the particles tends to decrease. For example, a decrease of the size is observed when the base is added to the reactives comparing to the opposite process [19].

The influence of temperature has also been studied by some reports. For the formation of magnetite nanoparticles, the number of particles decreases when the temperature increases [34].

3.2 Hydrothermal Methods

Hydrothermal synthesis methods have been reported to produce magnetite nanoparticles. In these methods, reactions are performed in aqueous media in reactors or autoclaves, and the temperature needs to be higher than 200 °C and the pressure needs to be higher than 2000 psi [35,36].

There are two main routes for the formation of ferrites via hydrothermal conditions: hydrolysis and oxidation or neutralization of mixed metal hydroxides. These two reactions are very similar, except that ferrous salts are used in the first method [37].

In the method, the solvent, temperature and time have great effects on the particles [38]. The size of the particles increases when the time of the reaction increases and also when the amount of water increases. The formation of the particles also has two steps: nucleation and crystal growth. At higher temperatures, the nucleation process is

faster than the crystal growth, so the size of the particles decreases. At longer reaction time, the crystal growth dominates, so larger particles are formed. Magnetite nanoparticles with size 27 nm have been produced by hydrothermal method, and bis(2-ethylhexyl) sulfosuccinate sodium salt are used as a surfactant [39].

3.3 High-temperature Decomposition of Organic Precursors

The decomposition of iron precursors in the presence of hot organic surfactants is able to produce iron oxide nanoparticles with good size control, narrow size distribution, and good crystallinity, and the produced particles are also well dispersed [40]. The iron precursors include $Fe(Cup)_3$, $Fe(CO)_5$, or $Fe(acac)_3$. For example, the decomposition of iron carbonyl in the presence of octyl ether and oleic acid at 100 °C can produce iron oleate. Cooled to room temperature, $(CH_3)_3NO$ is added and the solution is refluxed [40]. The decomposition of iron pentacarbonyl in the presence of oleic acid and aging at 300 °C can produce magnetite nanoparticles with a very good crystallinity, and the size of particles is from 4 to 16 nm [40]. In this method, the size and shape of the particles are determined by the reaction time, temperature, precursors, concentration, ratios of the reactants, and solvent. The surfactant on the surfaces of the particles is used to stabilize the colloid solution.

The thermal decomposition of iron carbonyl in the presence of octyl ether and oleic acid and using consecutive aeration can produce hydrophobic magnetite nanoparticles with narrow size distribution [41].

The decomposition of iron acetylacetonate with 1,2-hexadecanediol in the presence of oleylamine and oleic acid at high temperature has been reported. The particles that are produced have a size ranging from 4 to 20 nm [42].

The thermal decomposition of iron oleate and iron pentacarbonyl in organic solvent at different temperatures can produce particles with size ranging from 4 to 11nm [43].

The iron oxide nanoparticles produced are dispersible in some organic solvents, but most of them are not dispersible in water. The decomposition of $Fe(acac)_3$ or $FeCl_3$ in refluxing 2-pyrrolidone can produce water-dispersible particles in acidic or basic media [44,45]. 2-pyrrolidone has a good coordination capacity with metal ions, so it is not only a solvent with high boiling temperature but also a stabilizer. In the report, the size of the particles can be 4, 12, and 60 nm according to different reflux time [44]. In another report about the decomposition of $Fe(acac)_3$ in high boiling organic solvent, the particles with size of 4, 6, 9, and 12 nm are produced. These particles have a very narrow size distribution, and they are coated by 2,3-dimercaptosuccinic acid and are dispersible in water [46].

Recently, the decomposition of $Fe_3(CO)_{12}$ in the presence of oleic acid and diethylene glycol diethyl ether has been reported. The produced particles are then annealed at 300, 700, and 900 °C. The annealing temperature helps to control the size, size distribution, composition, and magnetic properties of the particles [47].

3.4 Sol-Gel Methods

The sol-gel process is a wet-chemical technique, and it is based on the hydrolysis and condensation of precursors in a colloidal solution (sol). A metal oxide network (gel) is formed by solvent removal or chemical reaction. A colloidal gel is produced by basic catalysis; a polymeric form of the gel is produced by acid catalysis [48].

The rates of hydrolysis and condensation are very important parameters in the method, and it largely influence the properties of particles produced. The lower and more controlled hydrolysis rate can produce smaller particles. The size of the particles is also related to the solvent, concentration, pH, and temperature [49].

After a heat treatment of the gel at 400 °C, γ-Fe_2O_3 particles with size ranging from 6 to 15 nm are formed [50]. The method allows the predetermination of the structure of the particles according to the experimental conditions. Using this method, γ-Fe_2O_3 nanoparticles can be coated in an inert, inorganic, transparent, and temperature-resistant silica matrix [51,52].

In most methods, to produce iron oxide-silica composites, iron oxide precursors need to be mixed with silica precursors in a solvent to form a sol [53-55]. The iron oxide-silica aerogel composites that are produced by sol-gel method are more reactive than conventional iron oxide [48]. The increase in reactivity is because of the large surface area of the particles supported on the silica aerogel [56].

Fe_xO_y-SiO_2 nanoparticles have been produced using alkoxide and aqueous routes [57]. The influence of some different silica precursors on the properties of the final particles has been studied.

3.5 Microemulsions

A microemulsion is defined as a thermodynamically stable isotropic dispersion of two immiscible liquids, since the nanosized domain of either or both liquids has been stabilized by an interfacial film of surface-active molecules [58]. In water-in-oil microemulsion systems, the microdroplets of the aqueous phase surrounded by surfactant molecules are dispersed in a continuous oil phase [59]. The surfactant molecules limit the nucleation, growth, and agglomeration of the particles [60]. When an iron salt solution is added to the microemulsion, the iron salt will be contained in the aqueous microdroplets. This microdroplets will continuously collide, coalesce, and break again [61]. Therefore, if two reactants are added in microemulsion, the precipitate of the resultant will be formed. The growth of the particles is a progress of interdroplet exchange and nuclei aggregation [62, 63]. The precipitate can be extract from the surfactants.

Using aqueous core with aerosol-OT/n-hexane reverse micelles in microemulsion has produced the iron oxide nanoparticles with a very small size distribution (Figure 3.4) [64]. The aqueous core is used to dissolve reactants. In the report, the solution of Fe^{3+} and Fe^{2+} salts with ratio 2:1 was dissolved in the aqueous core. A deoxygenated solution of sodium hydroxide is used to achieve precipitation. The magnetite nanoparticles with smaller size and narrower size distribution have been produced in the presence of nitrogen gas at low temperature (Figure 3.5) [65]. Due to the very small size (nanometer range) of the aqueous core, the particles formed usually have a size less than 15 nm and a very narrow size distribution (Figure 3.6). The biggest advantage of the microemulsion method is that it can control the size of the particles by controlling the size of the aqueous core [66].

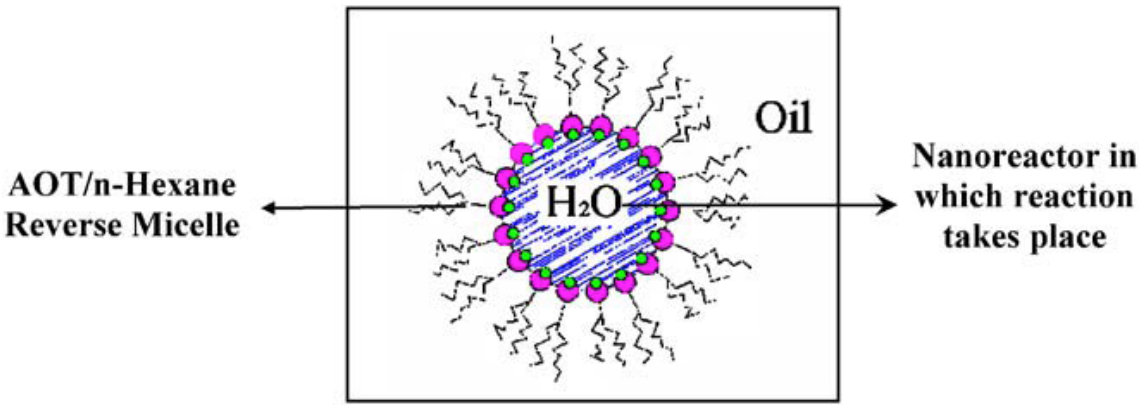

Figure 3.4 The structure of an aqueous core with aerosol-OT/n-hexane reverse micelles [64].

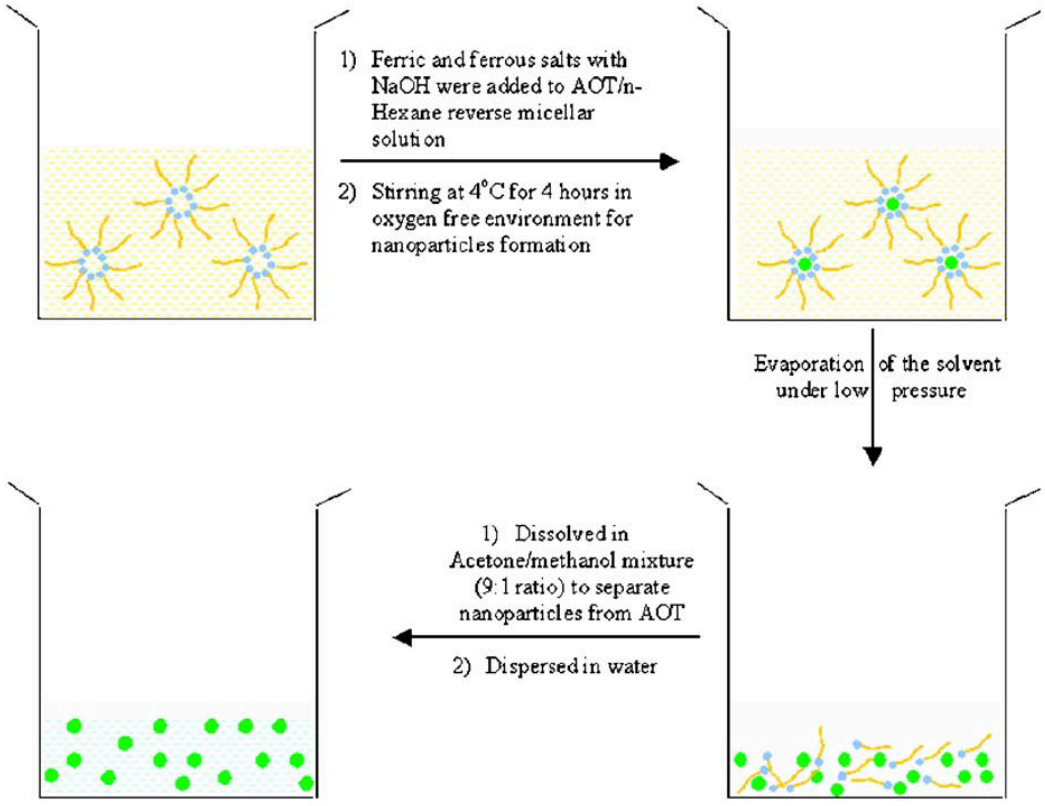

Figure 3.5 The microemulsion method producing highly monodispersed iron oxide nanoparticles [65].

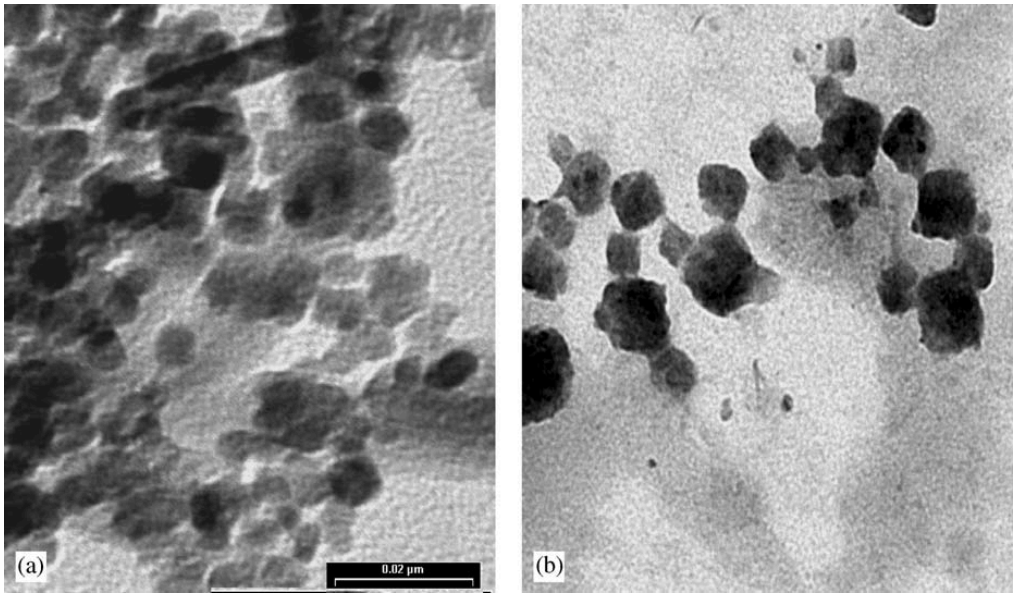

Figure 3.6 Transmission electron microscopy pictures of magnetic particles prepared in (a) bulk solutions and (b) in w/o microemulsions [21].

3.6 Polyol Methods

The iron oxide nanoparticles can be produced by the reduction of dissolved iron slats and direct precipitation in the presence of polyol [67, 68].

The polyols, such as polyethyleneglycol, have some good properties, such as the high dielectric constant, the ability to dissolve inorganic compounds, and the high boiling temperatures. They offer a wide range of the operating temperature for the production of inorganic compounds [69]. They are used not only as the agents of reduction but also as the stabilizers, and they can control the growth of particles and prevent aggregation.

In polyol method, precursor is suspended in a liquid polyol. The suspension is stirred and heated to a given temperature that reaches the boiling point of polyol. The precursor becomes soluble in the diol during the process, and then it reduced to form

metal nuclei that will form metal particles. The particles with desired size and shape can be produced by controlling the kinetic of the process.

The yield of iron oxide nanoparticles produced by this method depends on the type of polyols, ferrous salts, concentration, and temperature. The size and yield of the particles are related to the reduction potential of the polyols [70].

In one report, the non-aggregated magnetite nanoparticles have been produced by a modified polyol method [71]. Four different polyols, including ethylene glycol, diethyleneglycol, triethylene glycol, and tetraethylene glycol, are used to react with $Fe(acac)_3$ at an elevated temperature. The non-aggregated magnetite nanoparticles with narrow size distribution and uniformed shape are only produced when using triethylene glycol.

3.7 Electrochemical Methods

The γ-Fe_2O_3 nanoparticles with size ranging from 3 to 8 nm have been produced by electrochemical method [72]. In the method, the particles are produced from an iron electrode in an aqueous solution of dimethylformamide and cationic surfactant. The size of the particles is controlled by the current density.

Electrochemical deposition can be used to produce Fe_2O_3 and Fe_3O_4 particles under oxidizing conditions [73].

3.8 Aerosol/Vapor Method

Aerosol methods, including spray and laser pyrolysis, are continuous chemical processes, and they are allowing for high rate production.

Spray pyrolysis is a process that a solution of ferric salts and a reducing agent in organic solvents is sprayed into a series of reactors, where the solvent evaporates and the solute condenses [74]. The size of the original droplets controls the size of the produced particles. Using different iron precursors in alcoholic solution can produce maghemite particles with size ranging from 5 to 60 nm and with different shapes [75].

Laser pyrolysis is a good method to reduce the reaction volume. In the method, laser is used to heat a flowing gaseous mixture of iron precursor, and non-aggregated particles with small size and narrow size distribution can be produced. By controlling the experimental conditions, maghemite particles produced can have a size ranging from 2 to 7 nm and a very narrow size distribution [76, 77]. For example, maghemite nanoparticles with a size of 5nm have been produced by continuous laser pyrolysis of $Fe(CO)_5$ vapors [78].

3.9 Sonolysis

The decomposition of organometallic precursors by sonolysis can also produce iron oxide nanoparticles. Polymers, organic capping agents, or structural hosts can help to limit the particle growth [79,80]. The rapid collapse of sonically generated cavities generates very high temperature hot spot, which allows the conversion of ferrous salts into magnetic nanoparticles. For example, a hydrosol of amorphous magnetite nanoparticles can be produced by the sonolysis a of $Fe(CO)_5$ aqueous solution in the presence of sodium dodecyl sulfate [81].

Well-defined supermagnetic iron oxide nanoparticles have been produced by sonolysis [82]. In the report, the produced particles are coated with oleic acid, a

surfactant, and they can be dispersed in chitosan solution. The coated particles have a size of 65 nm, and they are very stable.

For applications, the particle size, size distribution, particles shape, and magnetic properties are the very important characteristics, and different characteristics of the particles can be obtained by different fabrication methods (Table 3.1).

Table 3.1 Comparison of Different Characteristics of the Iron Oxide Nanoparticles Produced by Different Fabrication Methods

Characteristics of the particles	**Bulk solution method**	**Aerosol/vapor method**	**Sol-gel method**	**Microemulsion method**
Size	2-50 nm	5-60 nm	6-200 nm	4-15 nm
Size distribution	Broad	Broad	Broad	Narrow
Morphology	Spherical (large aggregates)	Spherical	Spherical with high porosity	Cubic or spherical (no aggregation)
Magnetization	20-50 emu/g with superparamagnetic behavior	10-50 emu/g with desired magnetic property	10-40 emu/g with paramagnetic behavior	>30 emu/g with superparamagnetic behavior
Advantages	Large quantities can be synthesized	High production rate	Particles of desired shape and size can be synthesized, useful making hybrid nanoparticles	Uniform properties and size of the nanoparticles can be modulated
Disadvantages	Uncontrolled oxidation of maghemite, diamagnetic contribution	Large aggregatates are formed	Product usually contains sol-gel matrix components at their surfaces	Surfactants are difficult to remove, only a small quantities of iron oxide can be synthesized

CHAPTER 4

CHARACTERISTICS OF PARTICLES

4.1 Stability of Colloids

Iron oxide nanoparticles are prepared and stored in colloidal form, so the stability of the particles is very important. The stability of the particles is determined by three forces: hydrophobic-hydrophobic forces, magnetic forces, and van der Waals forces. The nanoparticles tend to aggregate due to the hydrophobic interactions, and micron clusters are formed from the aggregation. The micron clusters continue to aggregate due to the magnetic dipole-dipole interactions, and they are magnetized by neighboring clusters. In an external magnetic field, the clusters are further magnetized, and their aggregation increases [83]. The nanoparticles also aggregate in suspension due to van der Waals forces to minimize the total surface energy. The clusters have low surface areas, have large volumes, and show ferromagnetic behavior [83]. Therefore, the aggregation by these forces limits the applications of iron oxide nanoparticles.

Coatings (or stabilizer) are required to stabilize the iron oxide nanoparticles. Stabilizers, including surfactants and polymers, are usually added during the preparation process to prevent aggregation of the particles. For biomedical applications, the ideal coating materials also should be biocompatible and biodegradable. The polymers generally adhere to the surfaces in a substrate-specific manner [84]. Coatings also can protect the particles from further oxidization.

The electrostatic and steric repulsion are the two reasons of the stabilization [85]. The electrostatic force depends on the pH and ionic strength of the solution. The steric

repulsion is hard to predict, and, for polymer coatings, it depends on the molecular weight and density of the polymer.

The coating materials for the nanoparticles should be carefully chosen. The coating materials can be both inorganic and polymeric materials [86, 87]. The materials that have been used as coatings and their applications are listed in Table 4.1 [16].

Table 4.1 Coating Materials of Iron Oxide Nanoparticles and Their Applications [16]

Materials used	**Size and size distribution**	**Applications**	**Advantages**
Amorphous silica	20–200 nm, broad	Isolation of biomolecules, e.g. genomic and plasmid DNA, extraction of nucleic acids from soil, drug delivery, extraction of phenolic compounds from environmental water	Does not require any organic solvents and eliminates the need for the repeated centrifugation, vacuum filtration or column separation
Mesoporous silica	10–300 nm, broad	Controlled drug delivery, removal of mercury from industrial effluent, support for enzyme immobilization for bio-catalysis, fluorescence, isolation of genomic and plasmid DNA	Uniform pore size, large surface area, and high accessible pore volume
Polyethylene glycol (PEG)	10–50 nm, narrow	In vivo NMR imaging, in vivo contrasting	Improves the biocompatibility, blood circulation time and internalization efficiency of the NPs, easy to functionalize
Polyvinyl alcohol (PVA)	10–50 nm, narrow	In vivo imaging and drug delivery	Prevents coagulation of particles, giving rise to monodisperse particles
Polyvinyl pyrrolidine (PVP)	10–20 nm, narrow	Contrasting and drug delivery	Enhances the blood circulation time and stabilizes the colloidal solution
Polyacrylic acid	~250 nm, narrow	Target thrombolysis with recombinant tissue plasminogen activator	Increases the stability and biocompatibility of the particles and also helps in bioadhesion
Polystyrene	10–20 nm, narrow	Cellular imaging and DNA hybridization	Stable and uniform size particles in suspension
Polymethyl methacrylate	10–50 nm, narrow	DNA separation and amplification	Novel, simple and labor-saving; can be applied in automation system(s) to achieve high throughput detection of single nucleotide polymorphisms
Polydipyrrole/dicarbazole	20–100 nm, broad	DNA hybridization	Molecular diversity for engineering functional polyDPyr-/polyDCbz-shell outer layers of magnetic nanocomposites

Ethyl cellulose	20–50 nm, broad	Extraction of pharmaceutical chemicals	Enhanced the drug absorption into the surrounding tissues for a prolonged period of time
Chitosan	20–100 nm, broad	Tissue engineering, hyperthermia	A natural cationic linear polymer that is widely used as non-viral gene delivery system, biocompatible, hydrophilic, used in agriculture, food, medicine, biotechnology, textiles, polymers, and water treatment
Dextran	10–200 nm, narrow	Isolation of E. coli, drug delivery, imaging	Enhances the blood circulation time, stabilizes the colloidal solution
Starch	10–20 nm, narrow	Contrasting and imaging	Natural polymers, biocompatible
Liposome	50–200 nm, broad	Imaging, drug delivery, hyperthermia, contrasting	Long-circulating time
Albumin	100–200 nm, broad	Cell separation	Magnetic tagging and separation, does not affect cell viability and proliferation
Erythrocytes	10–100 nm, broad	MRI imaging, drug delivery	Avoids the rapid clearance by the reticuloendothelial system (RES) and permits a long half-life in blood circulation
Gelatin	50–100 nm	Isolation of genomic DNA, drug delivery	Hydrophilic, biocompatible, natural polymer. Improves the efficiency of drug loading and is a rapid, simple, and a well-suited method for DNA extraction

4.2 Characterization of Particles

The size and shape of iron oxide nanoparticles are also very important parameters because they are not only related to the magnetic properties but also related to the applications of the particles.

"Size" is not a clear concept. It can represent several different parameters. For example, size can represent the crystalline part of the iron core, the whole iron core including both the crystalline and amorphous part, the core, the whole particle including both the core and the coating, or even some value without a geometrical meaning. The particles also have a range of their size, so the size can represent the number, volume, or intensity-weighted mean size.

TEM can be used to characterize the size and shape of the particles [88]. By using TEM, the size of the particle core can be determined. It also provides the details of the size distribution and the shape of the particles (Figure 3.6). High-resolution TEM is also used to characterize the particles. It shows the arrangement of the atoms, so it can be used to study defects and surface atomic arrangement of the particles [89].

XRD can be used to determine the crystalline structure of the particles. In a XRD diffraction pattern, the intensity of the iron oxide peak can be used to determine the proportion of iron oxide formed in a mixture by comparing the experimental peak and reference peak intensities [90]. The size of the crystal can be determined from the line broadening in the XRD pattern using the Scherrer formula [91].

Small-Angle Neutron Scattering (SANS) can be used to characterize the size, size distribution, shape, and structure of the particles [92]. Dynamic light scattering (DLS) is used to determine the particle size [93].

The surface properties of coated iron oxide nanoparticles can be investigated by atomic force microscopy (AFM or CFM), secondary ion mass spectrometry (SIMS), infrared spectroscopy (IR), Fourier transform infrared spectroscopy (FTIR), X-ray photoelectron spectroscopy (XPS), thermogravimetric analysis (TGA), differential scanning calorimetry (DSC), thermal desorption spectroscopy (TDS), conductimetry, potentiometry, or solid-state nuclear magnetic resonance (SSNMR) [94]. These techniques are used to not only determine the nature and strength of the bonding between the iron oxide surface and the coating but also understand the effect of the coating on the magnetic properties of the particles [94].

4.3 Magnetic Properties of Colloids

The size of magnetic iron oxide particles needs to be much smaller than 1 μm in order to form a colloid suspension. Usually, the size is in the range of 4 nm to 18 nm, which is smaller than the size of a single domain. Therefore, all the magnetic moments in a particle are perfectly aligned, which means it is fully magnetized.

For a single domain nanoparticle, the magnetization is related to its anisotropy energy. The magnetic energy of a nanoparticle depends on the direction of its magnetization vector (Figure 4.1). The direction that has the minimum magnetic energy is call anisotropy direction or easy axes, and it depends on the crystal structure of the particle. The magnetic energy increases with the increase of the angle between the magnetization vector and the easy axis. The amplitude of this curve is called anisotropy energy.

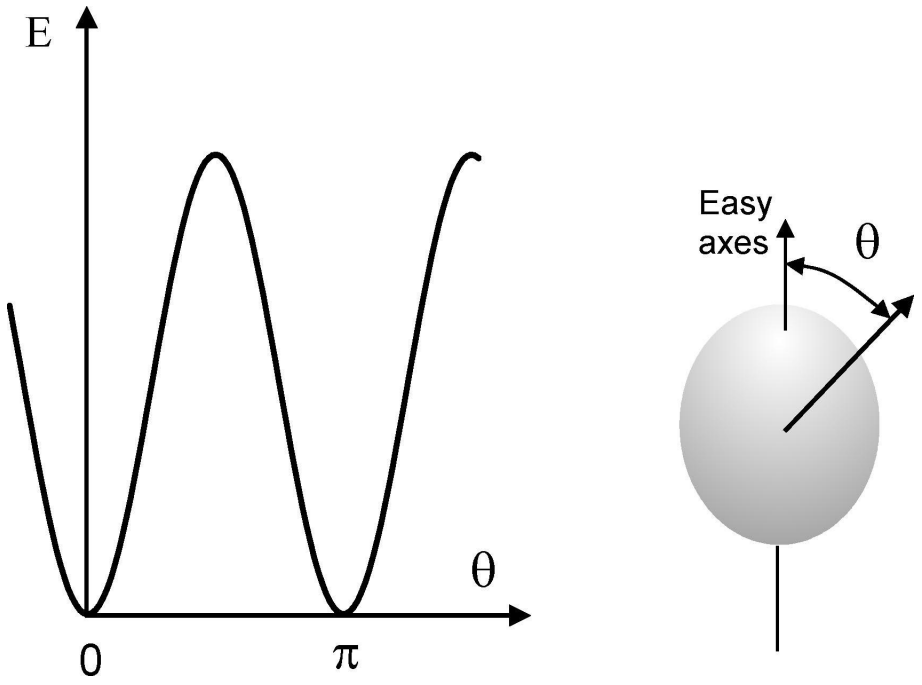

Figure 4.1 Changing of the magnetic energy with the angle between the magnetization vector and the easy axis [95].

Anisotropy energy is proportional to the volume of the particle, and it is given as:

$$E_a = K_a V$$

where E_a is the anisotropy energy, K_a is a constant called anisotropy constant, and V is the volume of the particle.

The Néel relaxation time also depends on the anisotropy energy. In Figure 4.1, the anisotropy energy gets its minimum value when $\theta = 0$ or π, that are the two easy axis. These two orientations that are antiparallel to each other have the lowest magnetic energy, so they are the stable states. Therefore, the magnetic moment in a single domain nanoparticle usually orients in these orientations that are separated by anisotropy energy barriers. At a finite temperature, there is a finite probability for the magnetization to jump over the energy barrier and reverse its direction. This process is called Néel relaxation,

and the mean time required for the jumps between different easy directions is called the Néel relaxation time, τ_N, and it is given as:

$$\tau_N = \tau_0 \exp(\frac{E_a}{kT})$$

where E_a is the anisotropy energy, k is the Boltzmann constant, T is the absolute temperature, and τ_0 is a length of time. τ_0 is also a function of the anisotropy energy, and it is given as:

$$\tau_0 = \frac{\sqrt{\pi}}{4} \frac{(M_s(0)V)}{E_a \gamma_e} \left[\frac{1}{\eta_f} + \eta_f \left(\frac{M_s(T)}{M_s(0)} \right)^2 \right] \sqrt{\frac{kT}{E_a}} \left(1 + \frac{kT}{E_a} \right)$$

where V is the volume of the particle, $M_s(0)$ is the specific magnetization of the particle at 0 K, $M_s(T)$ is the specific magnetization of the particle at absolute temperature T, γ_e is the gyromagnetic ratio of the electron, and η_f is a dimensionless constant and is given as:

$$\eta_f = \eta \gamma_e M_s(0)$$

where η is the damping constant.

According to the equations, τ_N increases when E_a increases; however, τ_0 decreases when E_a increases. For small anisotropy energy and high temperatures, $E_a << kT$, so the exponential factor is closed to 1. Therefore, the Néel relaxation time mainly depends on τ_0, which decreases as E_a increases. In contrast, for high anisotropy energy, $E_a >> kT$, so the Néel relaxation time mainly depends on the exponential factor. In this case, the Néel relaxation time increases rapidly with an increasing E_a. τ_0 is usually in the range between

10^{-10} and 10^{-9} seconds, and the Néel relaxation time can be anywhere from a few nanoseconds to years or much longer.

For the magnetic nanoparticles in a colloid, the return of the magnetization to equilibrium depends on not only the Néel relaxation but also the Brownian relaxation. Brownian relaxation represents the viscous rotation of the particles under a magnetic field (Figure 4.2). Thus, the global magnetic relaxation rate of the colloid is equal to sum of the Néel relaxation rate and the Brownian relaxation rate.

$$\frac{1}{\tau} = \frac{1}{\tau_N} + \frac{1}{\tau_B}$$

where τ is the global relaxation time and τ_B is the Brownian relaxation time, which is given as:

$$\tau_B = \frac{3V\eta}{kT}$$

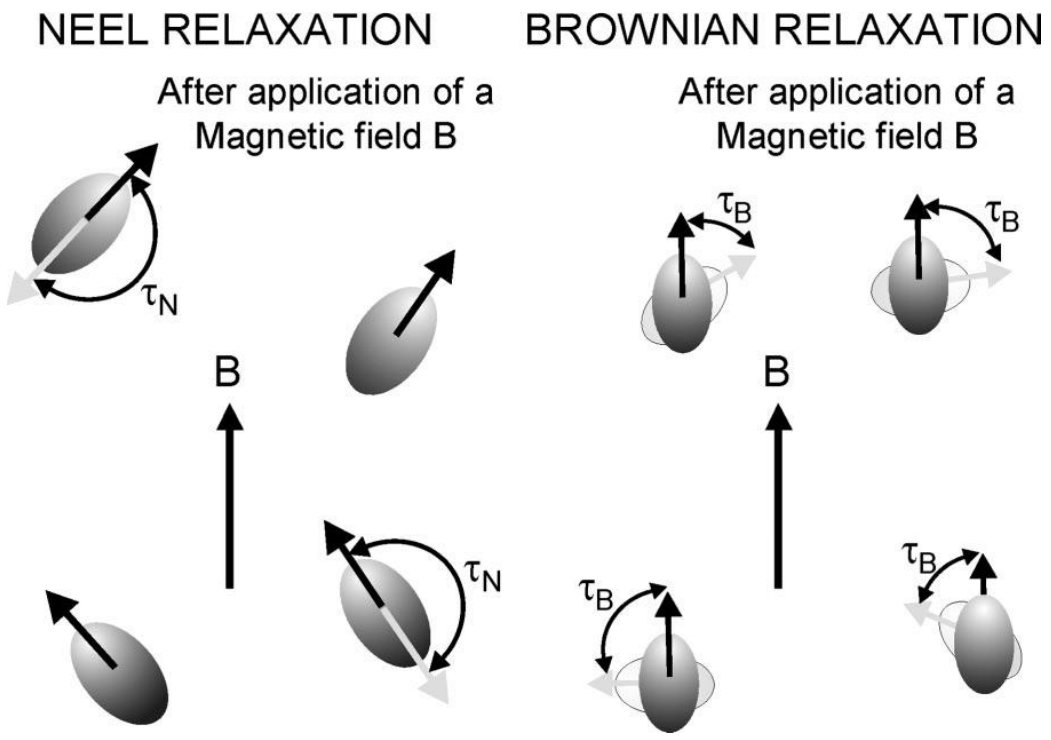

Figure 4.2 Illustration of the Néel relaxation and the Brownian relaxation in a colloid [96].

According to the equations, the Néel relaxation component dominates when the size of the particles is small, and the Brownian relaxation component dominates when the size of the particles is large. When the relaxation time is much shorter than the time used to measure the magnetization of the nanoparticles, the particles are superparamagnetic.

The blocking temperature is the temperature at which the magnetic relaxation time is equal to the measuring time. When the temperature is below the blocking temperature, a hysteresis can be observed. The blocking temperature is given as:

$$T_B = \frac{E_a}{k \ln\left(\frac{\tau_m}{\tau_0}\right)}$$

where T_B is the blocking temperature and τ_m is the measuring time. According to the equation, the blocking temperature increases with increase anisotropy energy.

CHAPTER 5

BIOMEDICAL APPLICATIONS

Small magnetic iron oxide particles have been used in in vitro diagnostics for nearly forty years [97]. Because of the unique physical, chemical, thermal, and mechanical properties of iron oxide nanoparticles, they have been used in a great number of biomedical applications (Figure 5.1).

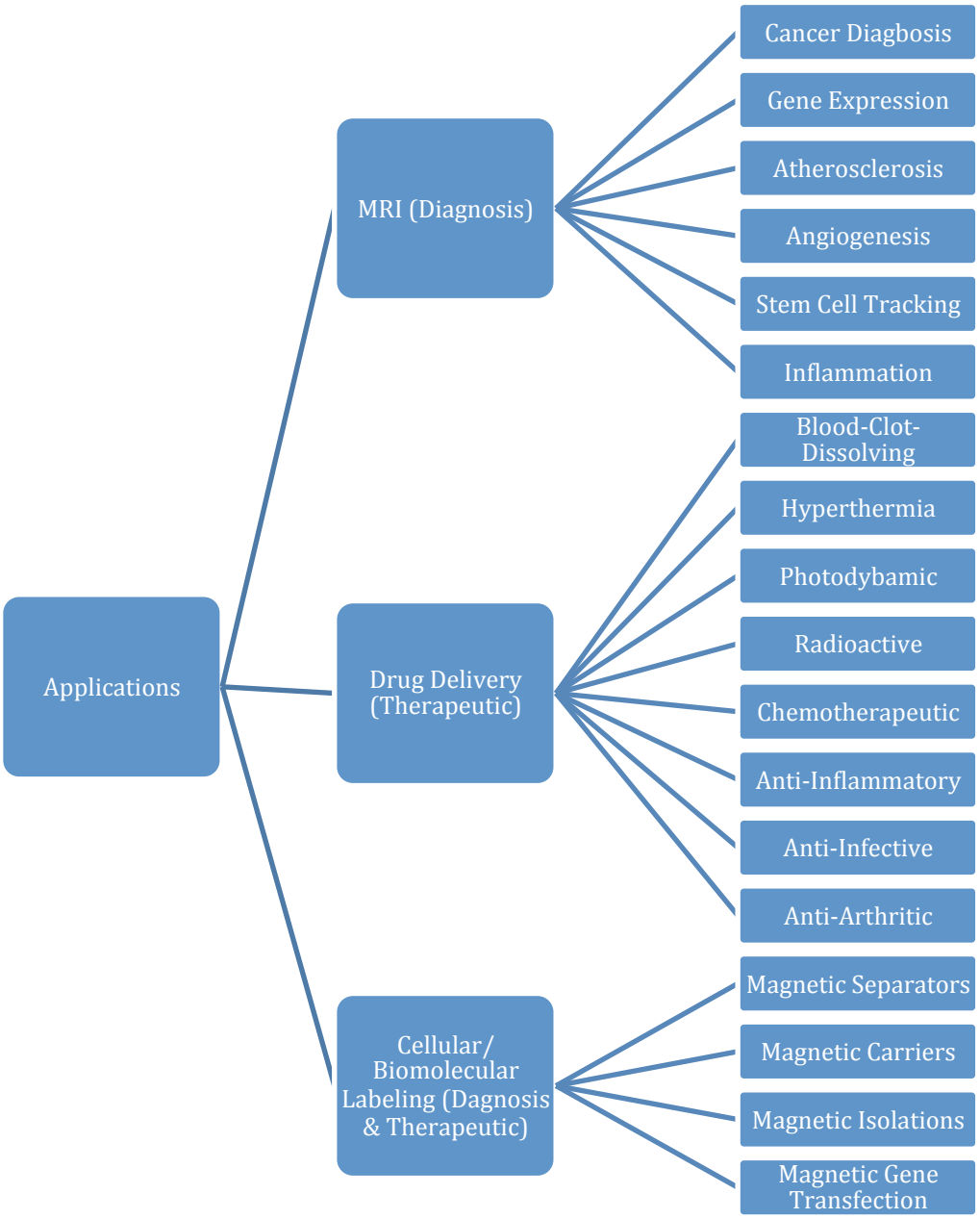

Figure 5.1 Recent biomedical applications of magnetic iron oxide nanoparticles.

Magnetite and magnetite nanoparticles have been used in a lot of biomedical applications because of their biocompatibility and low toxicity in human body [98]. They are used for the magnetic resonance imaging contrast agents, drug delivery vehicles, and immunoassays, and also in magnetic hyperthermia. All these applications require that the

particles are superparamagnetic at room temperature. Aggregation needs to be avoided to prevent the blockage of blood vessels. In addition, the stability of the particles in water at neutral pH is very important for the applications, and the colloidal stability of the magnetic fluid is related to the coating materials and the size of the particles.

In the application of MRI, superparamagnetic iron oxide nanoparticles are used as contrast agents in human body for molecular and cell imaging to better differentiate between healthy and diseased tissue. By using the contrast agents, the resolution of the MRI in vivo imaging can be microscopic [99].

In the application of drug delivery, superparamagnetic iron oxide nanoparticles are used as carriers of drugs, which means drugs bear on the surface or in the bulk of the particles. In an applied external magnetic field, the particles are driven to the desired region in the body, and the medication can be released locally. This method allows the reduction of the drug wastage and side effects [100].

Magnetic iron oxide nanoparticles are also used for hyperthermia in cancer therapy. Superparamagnetic nanoparticles can be used to heat tumor cells to 41-45 °C in an alternating magnetic field. The damage for normal tissue is reversible, but the damage for the tumor cells is irreversible [11].

Magnetic iron oxide nanoparticles with polymer coatings have been also used in cell separation, protein purification, and organic and biochemical syntheses. The coatings are not only used to enhance the stability but also the functionality of the particles.

All the applications listed above have requirements on the size, size distribution, shape, structure, chemical composition, and coating material of the particles, and these

factors are all determined by the preparation method. Therefore, different synthesis processes are used for different applications.

For most of these applications, the magnetic behavior of iron oxide nanoparticles in fluid is a very important topic, especially, the high gradient magnetic separation of the particles from a nonmagnetic liquid medium, such as blood in the human body, in an external magnetic field. Many biomedical applications, such as drug delivery, cell separation, and protein purification, and industrial applications, such as ore refinement and water treatment, are based on this model.

CHAPTER 6

MAGNETIC IRON OXIDE NANOPARTICLES IN FLUIDS

6.1 Model

In this thesis, a simple 2D model, which represents a slice through the center of a spherical particle in a fluid, is considered (Figure 6.1). The fluid flows in a channel, and a magnetic field is applied perpendicular to the channel walls. The particle is attracted toward the wall by the magnetic force and will be captured at the inner surface of the wall. The superparamagnetic nanoparticle in this model consists of a single domain crystalline core and a coating layer. The coordinate origin sets at the bottom of the channel.

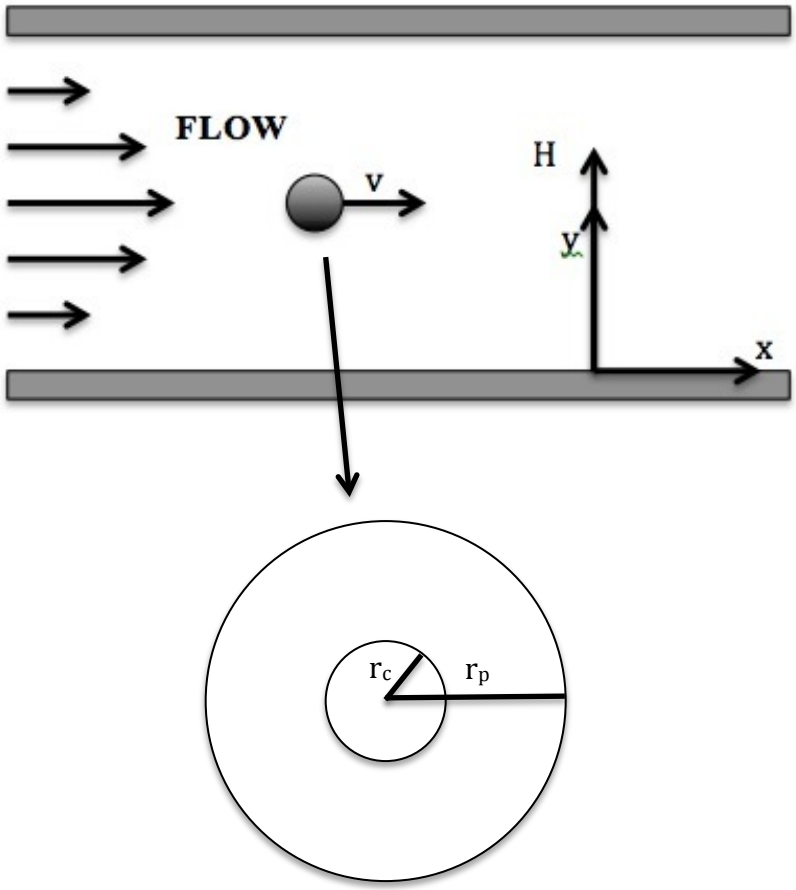

Figure 6.1 Schematic diagram of the model.

6.2 The Forces and Trajectory

To separate the particle from the fluid, the magnetic force on the particle must overcome the opposing forces, including fluid drag, gravitational, and inertial forces. In this case, since the size of the particle is in nanoscale, only the influence of the magnetic and drag forces are considered.

By definition, the magnetic force can be written as:

$$F_m = m \cdot \nabla B = \mu_0 V_c M_c \cdot \nabla H$$

where m is the magnetic moment of the particle, μ_0 is the permeability of free space, V_c is the volume of the core, M_c is the magnetization of the core, and H is the magnetic field. The magnetization of the core of the superparamagnetic nanoparticle is proportional to the Langevin function.

$$M_c = Np_m L(x)$$

where N is the number of atoms per unit volume, p_m is the magnetic dipole moment per atom, and L(x) is the Langevin function, which is given as:

$$L(x) = \coth(x) - \frac{1}{x}$$

with

$$x = \frac{\mu_0 p_m H}{kT}$$

where k is the Boltzmann constant and T is the temperature. By definition,

$$\chi = \frac{\mu_0 N p_m^2}{3kT}$$

where χ is the magnetic susceptibility.

From all the equations above, the relation can be derived as:

$$M_c = \frac{3\chi}{\chi + 3} H$$

so

$$F_m = \frac{3\mu_0 V_c \chi}{\chi + 3} \cdot \nabla H^2$$

According to the equation above, the magnetic force toward the bottom of the channel is proportional to the volume of the particle core, the magnetic field gradient, and the magnetic field at the location of the particle. It can also be written as:

$$F_m = \frac{4\pi\mu_0 r_c^3 \chi}{\chi + 3} \cdot \nabla H^2$$

where r_c is the radius of the particle core.

The other force in the fluid is the horizontal drag force, which exerts on the spherical particle, so it can be given by the Navier–Stokes equation:

$$F_d = 6\pi\eta r_p v_x$$

where η is the viscosity of the liquid medium, r_p is the radius of the whole particle, and v_x is the flow velocity at the center of the particle, which can be given as:

$$v_x = \frac{4v_{\max}}{D^2}(Dy - y^2)$$

where v_{max} is the maximum flow velocity at the center of the channel and D is the diameter of the channel. y is in the range between 0 and D . Therefore, the horizontal drag force can be finally written as:

$$F_d = \frac{24\pi\eta r_p v_{\max}}{D^2}(Dy - y^2)$$

According to the equation, the drag force is proportional to the radius of the particle and the velocity of the fluid.

The trajectory of the particle in the channel from the two forces exerting on the particle can be calculated. By applying Newton's law, the small displacement of the particle in y direction can be given as:

$$dy = -\frac{F_m}{F_d}dx$$

then

$$(y^2 - Dy)dy = \frac{\mu_0 r_c^3 D^2 \chi \nabla H^2}{6\eta r_p v_{\max}(\chi + 3)}dx$$

If the particle originally at the point (0,h), where h is in the range between 0 and D, the trajectory function of the particle can be derived by integrate both sides of the equation above.

$$\int_h^y (y^2 - Dy)\,dy = \int_0^x \frac{\mu_0 r_c^3 D^2 \chi \nabla H^2}{6\eta r_p v_{\max}(\chi + 3)}dx$$

then, the trajectory function can be written as:

$$2y^3 - 3Dy^2 - \frac{\mu_0 r_c^3 D^2 \chi \nabla H^2}{\eta r_p v_{\max}(\chi + 3)}x - 2h^3 + 3Dh^2 = 0$$

For this model, the equation above is the final form of the trajectory function, where h is in the range from 0 to D and y is in the range from 0 to h.

According to the equation, the trajectory of the particle in the fluid is related to the field gradient, diameter of the channel, size of the particle, and viscosity of the liquid medium.

6.3 Results

For most biomedical applications, the channel in the model represents blood vessel, and the liquid medium represents blood. Table 6.1 shows the values that are used in this simulation.

Table 6.1 The Values Used in the Simulation

Property	**Value**	**Unit**
η	0.002	kg m^{-1} s^{-1}
$\mu_0 H$	1	kg s^{-2} A^{-1}
dH/dy	$1*10^{10}$	A m^{-2}
χ	1000	
v_{max}	0.001	m s^{-1}
D	50	μm
r_c	$50*10^{-9}$	m
r_p	$1*10^{-6}$	m

Substituting these values into the trajectory function, then the function becomes:

$$2y^3 - 150y^2 - 1557.8x - 2h^3 + 150h^2 = 0$$

where the variables x and y have the unit of μm. Therefore, the trajectory of the particle in the blood vessel depends on the height, h, which the particle is originally at. Figure 6.2 shows the trajectories of the particle starting at different heights.

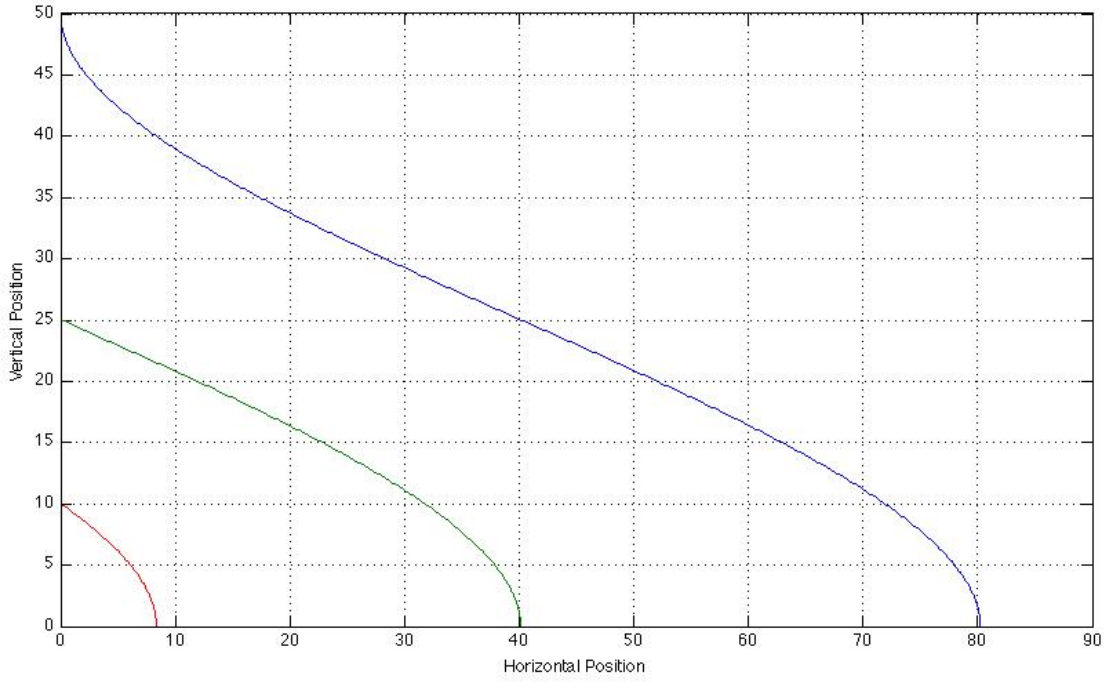

Figure 6.2 The trajectories of the particle starting at height 10, 25, and 50 μm, and the x and y axes have the unit of μm.

When y=0 or 50, the flow velocity v_x=0, so the curves have the biggest slope. When y=25, v_x= v_{max}, so the curves have the smallest slope. Using higher magnetic gradient or magnetic field, the particle can be captured in shorter distance and vice versa.

CHAPTER 7

CONCLUSIONS

The modern synthesis methods of the iron oxide nanoparticles allow not only the production of superparamagnetic particles with very narrow size distribution and the engineering of the surfaces of the particles with different functions. The applications of the particles strongly depend on the magnetic properties of the particles, and the magnetic properties of the particles strongly depend the size of the particles. Therefore, the synthesis methods of the particles are very important for applications. The biomedical applications of magnetic nanoparticles can provide better diagnostic procedures and better treatment modalities, therefore, the better quality of our lives.

The magnetic behavior of iron oxide nanoparticles in fluid is a very important topic for most of the applications, especially, the separation of the particles from a nonmagnetic liquid medium. For the model created in the thesis, only the magnetic force and the drag force are taken into consideration. The magnetization of the particle is calculated by using the Langevin function. The fluid drag force is calculated by using the Navier–Stokes equation. The trajectory of the particle in the fluid is related to the field gradient, diameter of the channel, size of the particle, and viscosity of the liquid medium. This model can be applied to many applications such as drug delivery, cell separation, protein purification, ore refinement, and water treatment.

REFERENCES

[1] R.M. Cornell, U. Schwertmann, The Iron Oxides: Structure, Properties, Reactions, Occurrences and Uses, second ed. Wiley-VCH, Weinheim, German, 2003.

[2] P. Majewski, B. Thierry, Critical Reviews in Solid State and Material Science 32 (3-4) (2007) 203-215.

[3] http://www.britannica.com/EBchecked/topic/356602/maghemite, accessed 03/2012.

[4] http://en.wikipedia.org/wiki/Iron_oxide_nanoparticles, accessed 03/2012.

[5] E. Murad, in: J.W. Stucki, B.A. Goodman, U. Schwertmann (Eds.), Series C: Mathematical and Physical Sciences. D. Reidel, 1985.

[6] S.P. Sena, R.A. Lindley, H.J. Blythe, C. Sauer, M. Al-Kafarji, G.A. Gehring, Journal of Magnetism and Magnetic Materials 176 (2-3) (1997) 111-126.

[7] T. Kado, Journal of Applied Physics 103 (4) (2008) 043902-1-043902-4.

[8] H. Qiu, L. Pan, L. Li, H. Zhu, X. Zhao, M. Xu, L. Qin, J.Q. Xiao, Journal of Applied Physics 102 (11) (2007) 113913-1-113913-5.

[9] D.T. Margulies, F.T. Parker, F.E. Spada, R.S. Goldman, J. Li, R. Sinclair, A.E. Berkowitz, Physical Review B 53 (14) (1996) 9175-9187.

[10] D.T. Margulies, F.T. Parker, M.L. Rudee, F.E. Spada, J.N. Chapman, P.R. Aitchison, A.E. Berkowitz, Physical Review Letters 79 (25) (1997) 5162-5165.

[11] T. Neuberger, B. Schopf, H. Hofmann, M. Hofmann, B. von Rechenberg, Journal of Magnetism and Magnetic Materials 293 (1) (2005) 483-496.

[12] R.H. Kodama, Journal of Magnetism and Magnetic Materials 200 (1999) 359.

[13] F.E. Spada, F.T. Parker, C.Y. Nakakura, A.E. Berkowitz, Journal of Magnetism and Magnetic Materials 120 (1-3) (1993) 129-135.

[14] F.E. Spada, A.E. Berkowitz, N.T. Prokey, Journal of Applied Physics 69 (8) (1991) 4475-4477.

[15] U. Jeong, X.W. Teng, Y. Wang, H. Yang, Y.N. Xia, Advanced Materials 12 (1) (2007) 33-60.

[16] M. Mahmoudi, S. Sant, B. Wang, S. Laurent, T. Sen, Advanced Drug Delivery Reviews 63 (2011) 24-46.

[17] Y. Zhao, Z. Qiu, J. Huang, Chinese Journal of Chemical Engineering 16 (3) (2008) 451-455.

[18] T.K. Indira, P.K. Lakshmi, International Journal of Pharmaceutical Sciences and Nanotechnology 3 (3) (2010) 1035-1042.

[19] R. Massart, V. Cabuil, Journal of Chemical Physics 84 (1987) 967.

[20] C.E. Sjogren, K. Briley-Saebo, M. Hanson, C. Johansson, Magnetic Resonance in Medicine 31 (3) (1994) 268-272.

[21] A.K. Gupta, M. Gupta, Biomaterials 26 (2005) 3995-4021.

[22] A.K. Gupta, A.S.G. Curtis, Biomaterials 25 (15) (2004) 3029-3040.

[23] D.K. Kim, Y. Zhang, W. Voit, K.V. Rao, M. Muhammed, Journal of Magnetism and Magnetic Materials 225 (1-2) (2001) 30-36.

[24] P. Tartaj, M.P. Morales, S. Veintemillas-Verdaguer, T. Gonzalez-Carreno, C.J. Serna, Handbook of Magnetic Materials, Elsevier, North-Holland, 2006, pp. 403.

[25] T. Sugimoto, E. Matijevic, Journal of Colloid and Interface Science 74 (1) (1980) 227-243.

[26] R. Massart, IEEE Transactions on Magnetics, 17 (1981) 1247.

[27] T. Sen, S. Magdassi, G. Nizri, I.J. Bruce, Miro & Nano Letters 1 (1) (2006) 39-42.

[28] J.P. Jolivet, C. Froidefond, A. Pottier, C. Chaeneac, S. Cassaignon, E. Tronc, P. Euzen, Journal of Materials Chemistry, 14 (21) (2004) 3281.

[29] J.P. Jolivet, L. Vassiere, C. Chaeneac, E. Tronc, E. Materials Research Society Symposium Proceedings, 432 (1997) 145.

[30] R. Massart, J. Roger, V. Cabuil, Brazilian Journal of Physics 2 (1995) 135.

[31] R. Massart, V. Cabuil, Journal of Chemical Physics (1987) 967.

[32] J.P. Jolivet, P. Belleville, E. Tronc, J. Livage, Clays and Clay Minerals 40 (1992) 531.

[33] X. Qui, J. Chin, Journal of Chemistry 18 (2000) 834.

[34] L. Babes, B. Denizot, G. Tanguy, J.J. Le Jeune, P. Jallet, Journal of Colloid and Interface Science 212 (2) (1999) 474.

[35] B. Mao, Z. Kang, E. Wang, S. Lian, L. Gao, C. Tian, C. Wang, Materials Research Bulletin 41 (2006) 2226.

[36] H. Zhu, D. Yang, L. Zhu, Surface and Coatings Technology 201 (2007) 5870.

[37] M.A. Willard, L.K. Kurihara, E.E. Carpenter, S. Calvin, V.G. Harris, Encyclopedia of Nanoscience and Nanotechnology, American Scientific Publishers, Stevenson Ranch, 2004, pp. 815.

[38] D. Chen, R. Xu, Materials Research Bulletin 33 (1998) 1015.

[39] Y.H. Zheng, Y. Cheng, F. Bao, Y.S. Wang, Materials Research Bulletin 41 (3) (2006) 525.

[40] T. Hyeon, S.S. Lee, J. Park, Y. Chung, H.B. Na, Journal of the American Chemical Society 123 (2001) 12798.

[41] K. Woo, J. Hong, J.P. Ahn, Journal of Magnetism and Magnetic Materials 293 (2005) 177.

[42] S. Sun, H. Zeng, D.B. Robinson, S. Raoux, P.M. Rice, S.X. Wang, G. Li, Journal of the American Chemical Society 126 (2004) 273.

[43] J. Park, E. Lee, N.M. Hwang, M. Kang, S.C. Kim, J.G. Huang, G. Park, H.J. Noh, J.H. Kim, J. Park, H. Hyeron, Angewandte Chemie International Edition, 44 (2005) 123.

[44] Z. Li, Q. Sun, M. Gao, Angewandte Chemie International Edition, 44 (1) (2004) 123.

[45] J. Wan, W. Cai, J. Feng, X. Meng, E. Liu, Journal of Materials Chemistry, 17 (2007) 1188.

[46] Y.W. Jun, Y.M. Huh, J.S. Choi, J.H. Lee, H.T. Song, S. Kim, S. Yoon, K.S. Kim, J.S. Shin, J.S. Suh, J. Cheon, Journal of the American Chemical Society 127 (16) (2005) 5732.

[47] D. Amara, I. Felner, I. Nowik, S. Margel, Colloids and Surfaces A: Physicochemical and Engineering Aspects 339 (2009) 106-110.

[48] U.T. Lam, R. Mammucari, K. Suzuki, N.R. Foster, Industrial and Engineering Chemistry Research 47 (3) (2008) 599-614.

[49] A. Tavakoli, M. Sohrabi, A. Kargari, Chemical papers 61 (3) (2007) 151-170.

[50] F.D. Monte, M.P. Morales, D. Levy, A. Fernandez, M. Ocana, A. Roig, E. Molins, K. O'Grady, C. Serna, Langmuir 13 (1997) 3627.

[51] D. Niznansky, J.L. Rehspringer, M. Drillon, IEEE Transactions on Magnetics 30 (1994) 821.

[52] F. Bentivegna, J. Ferré, M. Nyvlt, J.P. Jamet, D. Imhoff, M. Canva, A. Brun, P. Veillet. S. Visnovsky, F. Chaput, J.P. Boilot, Journal of Applied Physics 83 (1998) 7776.

[53] M. Tadic, D. Markovic, V. Spasojevic, V. Kusigerski, M. Remskar, J. Pirnat, Z. Jaglicic, Journal of Alloys and Componds 441 (1-2) (2007) 291-296.

[54] B. Heinrichs, L. Rebbouh, J.W. Geus, S. Lambert, H.C.L. Abbenhuis, F. Grandjean, G.J. Long, J.P. Pirard, R.A. van Santen, Journal of Non-Crystalline Solids 354 (2-9) (2008) 665-672.

[55] S.A. Corr, Y.K. Gun'ko, A.P. Douvalis, M. Venkatesan, R.D. Gunning, P.D. Nellist, Journal of Physical Chemistry C 112 (4) (2008) 1008-1018.

[56] C.T. Wang, S.H. Ro, Applied Catalysis A: General 285 (1-2) (2005) 196-204.

[57] M. Raileanu, M. Crisan, C. Petrache, D. Crisan, M. Zaharescu, Journal of Optoelectronics and Advanced Materials 5 (3) (2003) 693.

[58] R.P. Bagwe, J.R. Kanicky, B.J. Palla, P.K. Patanjali, D.O. Shah, Critical Reviews in Therapeutic Drug Carrier Systems 18 (1) (2001) 77-140.

[59] P. Tartaj, M.P. Morales, S. Veintemillas-Verdaguer, T.T. Gonzales-Carreno, J.C. Serna, Journal of Physics D: Applied Physics 36 (2003) 182-197.

[60] M.P. Pileni, Journal of Physical Chemistry 97 (27) (1993) 6961–6973.

[61] M.J. Lawrence, G.D. Rees, Advanced Drug Delivery Reviews 45 (1) (2000) 89-121.

[62] J.H. Fendler, Chemical Review 87 (1987) 877-899.

[63] T. Sugimoto, Advances in Colloid and Interface Science 28 (1987) 65.

[64] A.K. Gupta, S. Wells, IEEE Transactions on Nanobioscience 3 (1) (2004) 66-73.

[65] J. Tang, M. Myers, K.A. Bosnick, L.E. Brus, Journal of Physical Chemistry B 107 (2003) 7501-7506.

[66] N. Munshi, T.K. De, A. Maitra, Journal of Colloid and Interface Science 190 (2) (1997) 387-391.

[67] F. Fievet, J.P. Lagier, B. Blin, B. Beaudoin, M. Figlarz, Solid State Ionics 198 (1989) 32.

[68] V.K. Tzitzios, D. Petridis, I. Zafiropoulou, G. Hadjipanayis, D. Niarchos, Journal of Magnetism and Magnetic Materials 294 (2) (2005) 95.

[69] D. Jézéquel, J. Guenot, N. Jouini, F. Fiévet, Journal of Materials Research 10 (1995) 77.

[70] R.J. Joseyphus, D. Kodama, T. Matsumoto, Y. Sato, B. Jeyadevan, K. Tohji, Journal of Magnetism and Magnetic Materials 310 (2) (2007) 2393.

[71] W. Cai, J. Wan, Journal of Colloid and Interface Science 305 (2007) 366.

[72] C. Pascal, J.L. Pascal, F. Favier, M.L.E. Moubtassim, C. Payen, Chemical Materials 11 (1999) 141.

[73] H.R. Kahn, K. Petrikowski, Journal of Magnetism and Magnetic Materials 215-216 (2000) 526.

[74] C. Prcharroman, T. Gonzalez-Carreno, J.E. Iglesias, Physics and Chemistry of Minerals 22 (1995) 21.

[75] T. Gonzalez-Carreno, M.P. Morales, M. Gracia, C.J. Serna, Materials Letters 18 (1993) 151.

[76] S. Veintemillas-Vendaguer, M.P. Morales, O. Bomati-Miguel, C. Batista, X. Zhao, P. Bonville, R.P. Alejo, J. Ruiz-Cabello, M. Santos, J. Tendillo-Cortijo, J. Ferreiros, Journal of Physics 37 (2004) 2054.

[77] R. Alexandrescu, I. Morjan, I. Voicu, F. Dumitrache, L. Albu, I. Soare, G. Prodan, Applied Surface Science 248 (1-4) (2005) 138.

[78] M.C. Bautista, O. Bomati-Miguel, M.P. Morales, C.J. Serna, S. Veintemillas-Verdaguer, Journal of Magnetism and Magnetic Materials 293 (2005) 20-27.

[79] V.F. Puntes, K.M. Krishnan, A.P. Alivisatos, Topics in Catalysis 19 (2002) 145.

[80] H.G. Rotstein, R. Tannenbaum, Journal of Physical Chemistry B 106 (2002) 146.

[81] R.A. Mukh-Qasem, A. Gedanken, Journal of Colloid and Interface Science 284 (2) (2005) 489.

[82] E.H. Kim, H.S. Lee, B.K. Kwak, B.K. Kim, Journal of Magnetism and Magnetic Materials 289 (2005) 328.

[83] I.W. Hamley, Angewandte Chemie International Edition 42 (15) (2003) 1692-1712.

[84] G.D. Mendenhall, Y. Geng, J. Hwang, Journal of Colloid and Interface Science 184 (2) (1996) 519-526.

[85] R.M. Cornell, U. Schertmann, Iron Oxide in the Laboratory: Preparation and Charscterization, VCH Publishers, Weinheim, German, 1991.

[86] J. Yu, C.W. Lee, S.S. Im, J.S. Lee, Reviews on Advanced Materials Science 4 (2003) 55-59.

[87] L.M. Liz-Marzán, P.V. Kamat, Nanoscale Materials, Kluwer Academic Publishers, Boston, MA, 2003.

[88] R.Y. Hong, S.Z. Zhang, G.Q. Di, H.Z. Li, Y. Zheng, J. Ding, D.G. Wei, Materials Research Bulletin 43 (2008) 2457-2468.

[89] S. Brice-Profeta, M.A. Aeeio, E. Tronc, N. Menguy, I. Letard, C.C. Moulin, M. Nogue, C. Chaneac, J.P. Jolivet, P. Saintctavit, Journal of Magnetism and Magnetic Materials 288 (2005) 354.

[90] K. Inouye, R. Endo, Y. Otsuka, K. Miyashiro, K. Kaneko, T. Ishikawa, Journal of Physical Chemistry 86 (1982) 1465.

[91] S. Calvin, E.E. Carpenter, V.G. Harris, Physical Review B: Condensed Mater and Materials physics 6803 (3) (2003) 3411.

[92] P. Lindner, T.N. Zemb, X Ray and Light: Scattering Methods Applied to Soft Condensed Matter, Elsevier, North-Holland, 2002.

[93] N.D. Jaeger, H. Demeye, R. Findy, R. Sneyer, J. Vanderdeelen, P.V.D. Meeren, M. Laethem, Particle and Particle Systems Characterization 8 (1991) 179.

[94] M.D. Marco, I. Guilbert, M. Port, C. Robic, P. Couvreur, C. Dubernet, International Journal of Pharmaceutics 324 (1) (2006) 37.

[95] http://pubs.acs.org/action/showImage?doi=10.1021%2Fcr068445e&iName=master.img-014.jpg&type=master, accessed 03/2012.

[96] http://pubs.acs.org/action/showImage?doi=10.1021%2Fcr068445e&iName=master.img-015.jpg&type=master, accessed 03/2012.

[97] R.K. Gilchrist, R. Medal, W.D. Shorey, R.C. Hanselman, J.C. Parrot, C.B. Taylor, Annals of Surgery 146 (1957) 596-606.

[98] P. Majewski, B. Thierry, Critical Review in Solid State and Material Sciences 32 (3-4) (2007) 203-215.

[99] G.A. Jonson, Journal of Magnetic Resonance Q9 (1993) 1-30.

[100] A.S. Lubbe, C. Bergemann, H. Riess, F. Schriever, P. Reichardt, K. Possinger, M. Matthias, B. Dorken, F. Herrmann, R. Gurtler, P. Hohenberger, N. Haas, R. Sohr, B. Sander, A.J. Lemke, D. Ohlendorf, W. Huhnt, D. Huhn, Cancer Research 56 (20) (1996) 4686-4693.